

# Manifestation of unexpected semiconducting properties in few-layer orthorhombic arsenene

Zhiya Zhang, Jiafeng Xie, Dezheng Yang, Yuhua Wang, Mingsu Si\*, and Desheng Xue†

*Key Laboratory for Magnetism and Magnetic Materials of the Ministry of Education,*

*Lanzhou University, Lanzhou 730000, China*

(Dated: September 25, 2018)

## Abstract

In this express, we demonstrate few-layer orthorhombic arsenene is an ideal semiconductor. Due to the layer stacking, multilayer arsenenes always behave as intrinsic direct bandgap semiconductors with gap values of around 1 eV. In addition, these bandgaps can be further tuned in its nanoribbons. Based on the so-called acoustic phonon limited approach, the carrier mobilities are predicted to approach as high as several thousand square centimeters per volt-second and simultaneously exhibit high directional anisotropy. All these make few-layer arsenene promising for device applications in semiconducting industry.

Mainstream logic devices applications depend largely on high performance of semiconducting materials [1]. Graphene exhibiting superior carrier mobility seems to be an ideal candidate. On the other hand, the ability to control the electronic properties of a material by external field requires a moderate electronic bandgap [2]. Unfortunately, the intrinsic dispersion of graphene is gapless. Entire community still contributes to search for novel semiconducting materials. Recently, phosphorene, monolayer of black phosphorus (BP), is emerging as a promising two-dimensional (2D) semiconductor which might go beyond graphene. Phosphorene holds a high carrier mobility in a wide range of  $\sim 10^3$ - $10^4$   $\text{cm}^2\text{V}^{-1}\text{s}^{-1}$  [3, 4], and simultaneously maintains a considerable bandgap of around 2.0 eV [5]. At the same time, phosphorene and its bulk counterpart BP are stimulating intense fundamental researches owing to its versatile properties. For instance, structural transformations at high pressure [6], low-temperature superconducting [7], a highly anisotropic transport [8], excellent optical and thermoelectric responses [9], a negative Poisson's ratio [10], and strain-induced inversion of conduction bands [11] have been demonstrated. It is quite likely that these unusual properties make phosphorene potential for realization of optoelectronic devices in post-silicon era.

With five “*sp*” electrons in valence state, As sits below and closest to P in the periodic table. The condensed state substances of these two elements are most likely similar with each other from the chemical point of view. However, up to now, little is known for As compared to black phosphorene [12, 13]. On the other hand, following the success of graphene in experiments, various chemical classes of 2D materials initially considered to exist only in the realm of theory have been synthesized. Taking silicene as an example, it is first proposed through using *ab initio* method [14, 15] and then epitaxially grown on both silver (111) substrate [16] and diboride thin films [17] in experiments. All these motivate a timely study of As in low-dimensional forms, which would be promising for future device applications.

This express reports a large bandgap and a high carrier mobility simultaneously appearing in few-layer orthorhombic arsenic, based on first-principles calculations. The chemical symbol of As is the abbreviation of the word “arsenic”. Thereafter, a monolayer of As can be called “arsenene”, in analogy with graphene and phosphorene. Although the bandgap of the monolayer structure was reported to be indirect [12], our results surprisingly show that multilayer arsenenes always behave as intrinsic direct bandgap semiconductors with proper bandgaps around 1 eV. More importantly, the carrier mobilities are predicted to be as high

as several thousand square centimeters per volt-second. All these make few-layer arsenene intriguing for device applications in semiconducting industry.

The most stable configuration of As allotropes is the rhombohedral (A7) structure (called grey As). This is a metallic phase as bands near the T point and at the L point largely overlap by about 0.5 eV [18]. When it is heated at the boiling point of water ( $\sim 370$  K), an orthorhombic phase (arsenolamprite) arises as a similar structure to BP [19]. Owing to the less dense density compared with the A7 phase, the orthorhombic As is a narrow-band semiconductor with bandgap in the order of 0.3 eV [20]. In reality, little attention has been paid to the crystalline As in particular the orthorhombic one. The much sparser amorphous As with a gap of 1 eV or more takes up most of the research interest [21]. In this context, we focus our study on the orthorhombic As, as shown in Fig. 1(a). First Brillouin zone of the primitive cell is also displayed in Fig. 1(b). To guarantee the lattice parameters used accurately, five functionals are taken in realistic simulations (see Methods in Supporting Information (SI)) [22]. The optimized structural parameters are summarized in Tab. I. In comparison with the experiment [23], the revPBE-vdW functional [24] yields the reasonable lattice parameters which are slightly larger than the experimental ones. By contrast, the functional of PBE [25] without vdW correction produces a large error along the layer-stacking direction by as large as 4.1 percent. This means the vdW correction is of crucial importance in determining the interlayer distance. Generally, pure DFT underestimates the bandgap of a semiconductor because of the improper consideration of Coulomb interaction. The functional of revPBE-vdW gives a near zero bandgap at the Z point (see Fig. 1 in SI), contradicting the experiment measurement. To overcome this problem, the HSE06 hybrid functional [26] is utilized and the resultant band structure is displayed in Fig. 1(c). It clearly shows that orthorhombic As is an intrinsic direct bandgap semiconductor with bandgap of about 0.39 eV, comparable to the experimental value.

At the Z point, one valence band (VB) and one conduction band (CB) near the Fermi level disperse quite strongly along the Z-Q and Z- $\Gamma$  directions (Fig. 1(c)). As a result, very small effective masses of carriers can be highly expected. Based on the nearly free electron model, the effective mass of carrier can be evaluated as  $m^* = \hbar^2 / (\partial^2 E / \partial k^2)$  with  $\hbar$ ,  $E$ , and  $k$  being Planck's constant divided by  $2\pi$ , the band energy, and the crystal momentum, respectively. Using the above equation, almost equal effective masses of  $0.13 m_0$  (where  $m_0$  is the free-electron mass) are obtained for both electrons and holes along the Z-Q direction,

whereas those along the Z- $\Gamma$  direction are smaller ( $0.10 m_0$ ) for electrons and larger ( $0.26 m_0$ ) for holes. Relatively larger values are found along the direction Z-T'-A', where the carrier effective masses are  $1.26 m_0$  and  $1.70 m_0$  for electrons and holes, respectively. All these values are consistent with the experimental report [27]. Thus, such small effective masses obtained for orthorhombic As would set a crucial precondition for few-layer arsenene to exhibit a high carrier mobility, as discussed below.

In principle, arsenene can be fabricated through mechanically isolating the orthorhombic bulk counterpart. Here, we validate it by using first principles calculations, as shown in Fig. 2(a). Arsenene is indeed thermally stable since no imaginary frequency is observed in its phonon dispersion curve (see Fig. 2 in SI). In addition, we also check its stability from the cohesive energy. Although the cohesive energy of the grey As is more stable by about 0.15 eV/atom than that of orthorhombic one, the relatively smaller difference of around 0.01 eV/atom is obtained for their respective monolayers, indicating the possible existence of orthorhombic arsenene in experiments. The lattice parameters  $a = 4.80 \text{ \AA}$  and  $b = 3.68 \text{ \AA}$  are obtained for arsenene. Compared with the bulk phase, the lattice constant  $a$  is elongated by 2.8 percent in arsenene, while  $b$  is shortened by 0.8 percent. As a result, the bond angles  $\theta_1$  and  $\theta_2$  are changed accordingly, i.e.,  $\theta_1 = 100.92^\circ$  and  $\theta_2 = 94.52^\circ$ , leaving the bond lengths  $R_1 = 2.49 \text{ \AA}$  slightly decreased and  $R_2 = 2.51 \text{ \AA}$  nearly unchanged. Such modification in structural parameters stems from the lack of interlayer interactions when it goes from bulk to monolayer. However, the effect on electronic structure is huge, as discussed below.

The calculated band structure of arsenene is displayed in Fig. 2. It is interesting to note that arsenene is an indirect semiconductor with bandgap of  $\sim 0.90$  eV since the valence band maximum (VBM) and the conduction band minimum (CBM) occur at different crystal points  $x'$  and  $\Gamma$ . Our results are consistent with that reported by Kamal and Ezawa [12], except that our gap value is slightly larger by  $\sim 0.05$ - $0.07$  eV. This originates from the different structural parameters obtained from different functionals. Such an indirect bandgap in arsenene contrasts strikingly with phosphorene with a direct bandgap. To unveil this difference, we carefully check those structural parameters between them [4]. Two main changes occur for arsenene: (i) The bond lengths  $R_1$  and  $R_2$  increase by  $\sim 0.2 \text{ \AA}$  in arsenene, indicating the relatively weak covalent bonding of As-As compared with P-P; To still keep the stability, (ii) the bond angles  $\theta_1$  and  $\theta_2$  shrink by  $1.48$ - $2.59^\circ$ . We emphasize that this is a natural consequence as the heavier As atom behaves a weaker covalent characteristic

compared to P. This is also confirmed in the similar monolayer of antimony where the structural parameters largely change and the VB at the  $x'$  point significantly exceeds that at the  $\Gamma$  point (not shown for brevity), claiming an obvious indirect bandgap. To further understand the underlying physics, we map out the respective wavefunctions of VB and CB at the  $x'$  and  $\Gamma$  points, as shown in Fig. 2(c). Our findings are very insightful. For VBs, the bonding feature appears between the atoms linked by  $R1$  at the  $\Gamma$  point (see the first panel of Fig. 2(c)), while that at the  $x'$  point occurs between the atoms connected by  $R2$  (see the third panel of Fig. 2(c)). The mutual competition between them dictates the VBM. Obviously, in the case of arsenene, the VB at the  $x'$  point forms a weaker covalent bond and thus occupies the higher energy level. The opposite situation is found for CBs at the  $x'$  and  $\Gamma$  points. This is why arsenene is an indirect semiconductor.

Based on the above understanding, it is expected to realize the bandgap transition from indirect to direct via changing  $R1$  and  $R2$  accordingly. Layer stacking is demonstrated to be an effective approach in this express. Once any more layer is added, additional bands are introduced near the Fermi energy level. For example, at the  $\Gamma$  point, the bands VB1 and CB2 appear, as shown in Fig. 2(d). Due to the overlap of wavefunctions, VB1 and VB2 (CB1 and CB2) contribute to the bonding and antibonding states, respectively. However, the energy separations between those states are entirely different. At the  $\Gamma$  point, this value reaches as high as  $\sim 1$  eV for the conduction bands and about 0.5 eV for the valence bands, being obviously much larger than those at the  $x'$  point. This is because the  $p$  local orbital directly couples the neighbor layer at the  $\Gamma$  point, but not for the  $x'$  point. Such an overlap of interlayer  $p$  local orbitals not only makes the bonding length  $R1$  shorter, but also importantly pushes the bands CB1 and VB2 closer towards each other compared to those at the  $x'$  point. Thus, an indirect-direct bandgap transition is obtained at bilayer or multilayer, extending the potential applications of few-layer arsenene. This also explains why the orthorhombic bulk As is a direct bandgap semiconductor. Another effect of layer-stacking reflects in the decrease of bandgap, sharing the same mechanism proposed in our previous work [28]. As the layer increases, the fundamental bandgap decreases from 0.97 eV at monolayer to 0.16 eV at six-layer, as shown in Fig. 2(e). These bandgap values follow the exponential decay law (see the fitting dashed line). The limit bandgap obtained by extrapolation is around 0.16 eV (marked as Inf in Fig. 2(e)), larger than that we obtained for the bulk calculation. This is originated from the structural adjustment from bulk to

few-layer, as suggested by the changed structural parameters in few-layer arsenene (see Tab. I in SI). More accurate bandgaps of few-layer arsenene are obtained by the HSE06 hybrid functional, as shown by the red circles and dashed line in Fig. 2(e). While arsenene is of fundamental importance, practical applications involving this material may require only a small piece of it or a flake, but not in an infinite size. In this respect, their ribbons in nanometer scale with well-defined shape may be crucial for device applications. It is found that several armchair arsenene nanoribbons possess improved and tunable direct bandgaps following the quantum confinement effect [29] (see Fig. 3 in SI for more details).

In the following, we restrict our attention to carrier mobilities in few-layer arsenene. Based on the so-called acoustic phonon limited approach [30], the carrier mobility reads

$$\mu_{2D} = \frac{e\hbar^3 C_{2D}}{k_B T m^* m_a (E_l^i)^2}, \quad (1)$$

where  $e$  is the electron charge,  $\hbar$  is Plank's constant divided by  $2\pi$ ,  $k_B$  is Boltzmann's constant and  $T$  is the temperature.  $m^*$  ( $m_x^*$  or  $m_y^*$ ) is the effective mass in the transport direction and  $m_a$  is the averaged effective mass determined by  $m_a = \sqrt{m_x^* m_y^*}$ .  $E_l^i$  is the deformation potential constant of VBM for hole or CBM for electron along the transport direction, defined by  $E_l^i = \Delta V_i / (\Delta l / l_0)$ . Here  $\Delta V_i$  is the energy change of the  $i^{\text{th}}$  band under proper cell compression and dilatation,  $l_0$  is the lattice constant in the transport direction and  $\Delta l$  is the deformation of  $l_0$ . The elastic modulus  $C_{2D}$  of the longitudinal strain in the propagation directions (both  $x$  and  $y$ ) of the longitudinal acoustic wave is given by  $(E - E_0) / S_0 = C_{2D} (\Delta l / l_0)^2 / 2$ , where  $E$  is the total energy and  $S_0$  is the lattice volume at equilibrium for a 2D system.

Besides the effective mass, other two properties of the deformation potential and the 2D elastic modulus are also involved in the calculation of carrier mobility, as described in Eq. (1). First principles calculations based on the functional of revPBE-vdW are taken to yield these properties together with the carrier mobility, as illustrated in Tab. II. Since the VBM of the monolayer is located at the  $x'$  point but not at the  $\Gamma$  point (Fig. 2(b)), we neglect the discussion of electron mobility as listed in Tab. II for the monolayer. In the bilayer, the electron mobility exhibits a value of  $0.26\text{-}0.40 \times 10^3 \text{ cm}^2 \text{ V}^{-1} \text{ s}^{-1}$  along the  $\Gamma$ -X direction, being about four times higher than that along the  $\Gamma$ -Y direction. This triggers a strongly directional anisotropy, mainly caused by the relatively small effective mass and deformation potential. In addition, as the layer further increases, the electron mobility monotonously

increases and reaches  $2.17\text{-}2.66(0.45\text{-}0.51)\times 10^3 \text{ cm}^2\text{V}^{-1}\text{s}^{-1}$  along the  $\Gamma\text{-X(Y)}$  direction at six-layer. The directional anisotropy remains nearly unchanged. In the case of hole, in monolayer, the hole mobility of the  $\Gamma\text{-Y}$  direction is slightly larger than that of the  $\Gamma\text{-X}$  direction. But in multilayer, the  $\Gamma\text{-X}$  direction holds much higher hole mobilities, reaching as high as  $\sim 4\times 10^3 \text{ cm}^2\text{V}^{-1}\text{s}^{-1}$  at five-layer. This is a huge value if one remembers the typical carrier mobilities of  $200\text{-}500 \text{ cm}^2\text{V}^{-1}\text{s}^{-1}$  in  $\text{MoS}_2$  [31, 32]. Such a high hole mobility in few-layer arsenene benefits from the smaller deformation potential. The deformation potential reaches as small as  $\sim 1.7 \text{ eV}$  at four-layer, which is about two times smaller than the value of  $3.9 \text{ eV}$  in  $\text{MoS}_2$  [33]. It is also noticed that around 1-2 orders of magnitude smaller in hole mobilities are obtained along the  $\Gamma\text{-Y}$  direction, resulting in a large directional anisotropy of hole mobility. It is well known that the higher carrier mobility plays a crucial role in the performance of devices. Thus, few-layer arsenene with proper bandgaps and high carrier mobilities are potential for practical applications in semiconducting industry.

In conclusion, we have investigated the electronic properties of few-layer arsenene from first principles calculations. Our results show that few-layer arsenene possesses carrier mobilities as high as several thousand square centimeters per volt-second, which exhibits a high anisotropy. Combining such superior carrier mobilities with the tunable bandgaps around  $1 \text{ eV}$ , few-layer arsenene is an ideal semiconducting material for device applications in semiconducting industry.

We thank Dr. Wei Ji (RUC) for valuable communications. This work was supported by the National Basic Research Program of China under Grant No. 2012CB933101 and the National Science Foundation under Grant No. 51372107, No. 11104122 and No. 51202099. We also acknowledge this work as done on Lanzhou University's high-performance computer Fermi.

\* sims@lzu.edu.cn

† xueds@lzu.edu.cn

- 
- [1] Y. Cui, Z. Zhong, D. Wang, W. U. Wang, and C. M. Lieber, *Nano Lett.* **3**, 149 (2003).  
 [2] K. S. Novoselov, A. K. Geim, S. V. Morozov, D. Jiang, Y. Zhang, S. V. Dubonos, I. V. Grigorieva, and A. A. Firsov, *Science* **306**, 666 (2004).

- [3] L. Li, Y. Yu, G. J. Ye, Q. Ge, X. Ou, H. Wu, D. Feng, X. H. Chen, and Y. Zhang, *Nat. Nanotech.* **9**, 372 (2014).
- [4] J. Qiao, X. Kong, Z.-X. Hu, F. Yang, and W. Ji, *Nat. Commun.* **5**, 4475 (2014).
- [5] L. Liang, J. Wang, W. Lin, B. G. Sumpter, V. Meunier, and M. Pan, *Nano Lett.* **14**, 6400 (2014).
- [6] J. C. Jamieson, *Science* **139**, 1291 (1963).
- [7] J. Wittig and B. T. Matthias, *Science* **160**, 994 (1968).
- [8] H. Liu, A. T. Neal, Z. Zhu, Z. Luo, X. Xu, D. Tomáek, and P. E. Ye, *ACS Nano* **8**, 4033 (2014).
- [9] R. Fei, A. Faghaninia, R. Soklaski, J.-A. Yan, C. Lo, and L. Yang, *Nano Lett.* **14**, 6393 (2014).
- [10] J.-W. Jiang and H. S. Park, *Nat. Commun.* **5**, 4727 (2014).
- [11] R. Fei and L. Yang, *Nano Lett.* **14**, 2884 (2014).
- [12] C. Kamal and M. Ezawa, arXiv:1410.5166v1.
- [13] J. Han, J. Xie, Z. Zhang, D. Yang M. Si, and D. Xue, to be published in *Appl. Phys. Exp.*
- [14] K. Takeda and K. Shiraishi, *Phys. Rev. B* **50**, 14916 (1994).
- [15] S. Cahangirov, M. Topsakal, E. Aktürk, H. Sahin, and S. Ciraci, *Phys. Rev. Lett.* **102**, 236804 (2009).
- [16] P. Vogt, P. D. Padova, C. Quaresima, J. Avila, E. Frantzeskakis, M. C. Asensio, A. Resta, B. Ealet, and G. L. Lay, *Phys. Rev. Lett.* **108**, 155501 (2012).
- [17] A. Fleurence, R. Friedlein, T. Ozaki, H. Kawai, Y. Wang, and Y. Yamada-Takamura, *Phys. Rev. Lett.* **108**, 245501 (2012).
- [18] J. H. Xu, E. G. Wang, C. S. Ting, and W. P. Su, *Phys. Rev. B* **48**, 17271 (1993).
- [19] H. Krebs, W. Holz, and K. H. Worms, *Chem. Ber.* **90**, 1031 (1957).
- [20] G. N. Greaves, S. R. Elliott, and E. A. Davis, *Advances in Physics* **28**, 49 (1979).
- [21] W. B. Pollard and J. D. Joannopoulos, *Phys. Rev. B* **19**, 4217 (1979).
- [22] See Supporting Information at <http://iopscience.iop.org>.
- [23] P. M. Smith, A. J. Leadbetter, and A. J. Apling, *Philos. Mag. B* **31**, 57 (1975).
- [24] M. Dion, H. Rydberg, E. Schröder, D. C. Langreth, and B. I. Lundqvist, *Phys. Rev. Lett.* **92**, 246402 (2004).
- [25] J. P. Perdew, K. Burke, and M. Ernzerhof, *Phys. Rev. Lett.* **77**, 3865 (1996).
- [26] J. Heyd, G. E. Scuseria, and M. Ernzerhof, *J. Chem. Phys.* **118**, 8207 (2003).

- [27] O. S. Cooper and A. W. Lawson, *Phys. Rev. B* **4**, 3261 (1971).
- [28] J. Xie, Z. Y. Zhang, D. Z. Yang, D. S. Xue, and M. S. Si, *J. Phys. Chem. Lett.* **5**, 4073 (2014).
- [29] J. Xie, M. S. Si, D. Z. Yang, Z. Y. Zhang, and D. S. Xue, *J. Appl. Phys.* **116**, 073704 (2014).
- [30] K. Kaasbjerg, K. S. Thygesen, and A.-P. Jauho, *Phys. Rev. B* **87**, 235312 (2013).
- [31] R. Fivaz and E. Mooser, *Phys. Rev.* **163**, 743 (1967).
- [32] B. Radisavljevic, A. Radenovic, J. Brivio, V. Giacometti, and A. Kis, *Nat. Nanotech.* **6**, 147 (2011).
- [33] K. Kaasbjerg, K. S. Thygesen, and K. W. Jacobsen, *Phys. Rev. B* **85**, 115317 (2012).

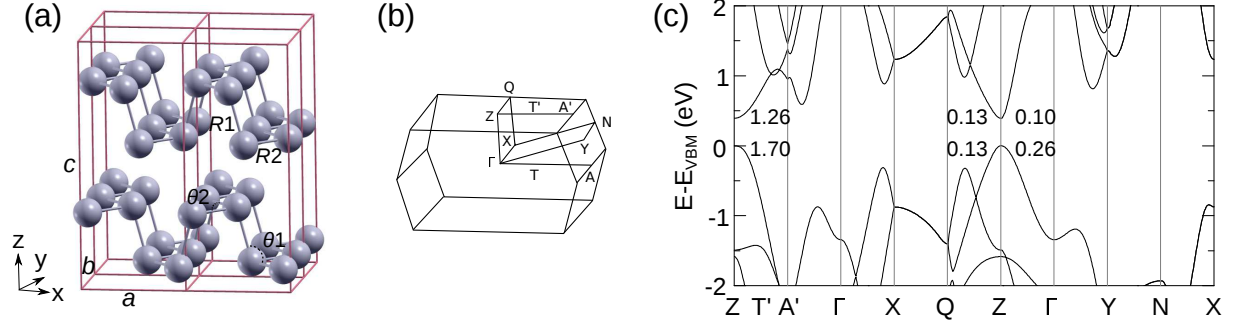


FIG. 1: (color online) (a) The conventional crystal structure of orthorhombic bulk As. The lattice constants  $a$ ,  $b$ , and  $c$  and the internal parameters  $R1$ ,  $R2$ ,  $\theta1$ , and  $\theta2$  are given as well. A  $2 \times 2 \times 1$  supercell is taken for clarity. (b) First Brillouin zone of primitive unit cell. The high-symmetry lines and points are given as well. (c) Band structure for orthorhombic As calculated using the HSE06 hybrid functional under the revPBE-vdW functional optimized structure. The fitted effective masses are given along the Z-T'-A', Z-Q, and Z- $\Gamma$  directions.  $E_{VBM}$  is the energy of valence-band maximum.

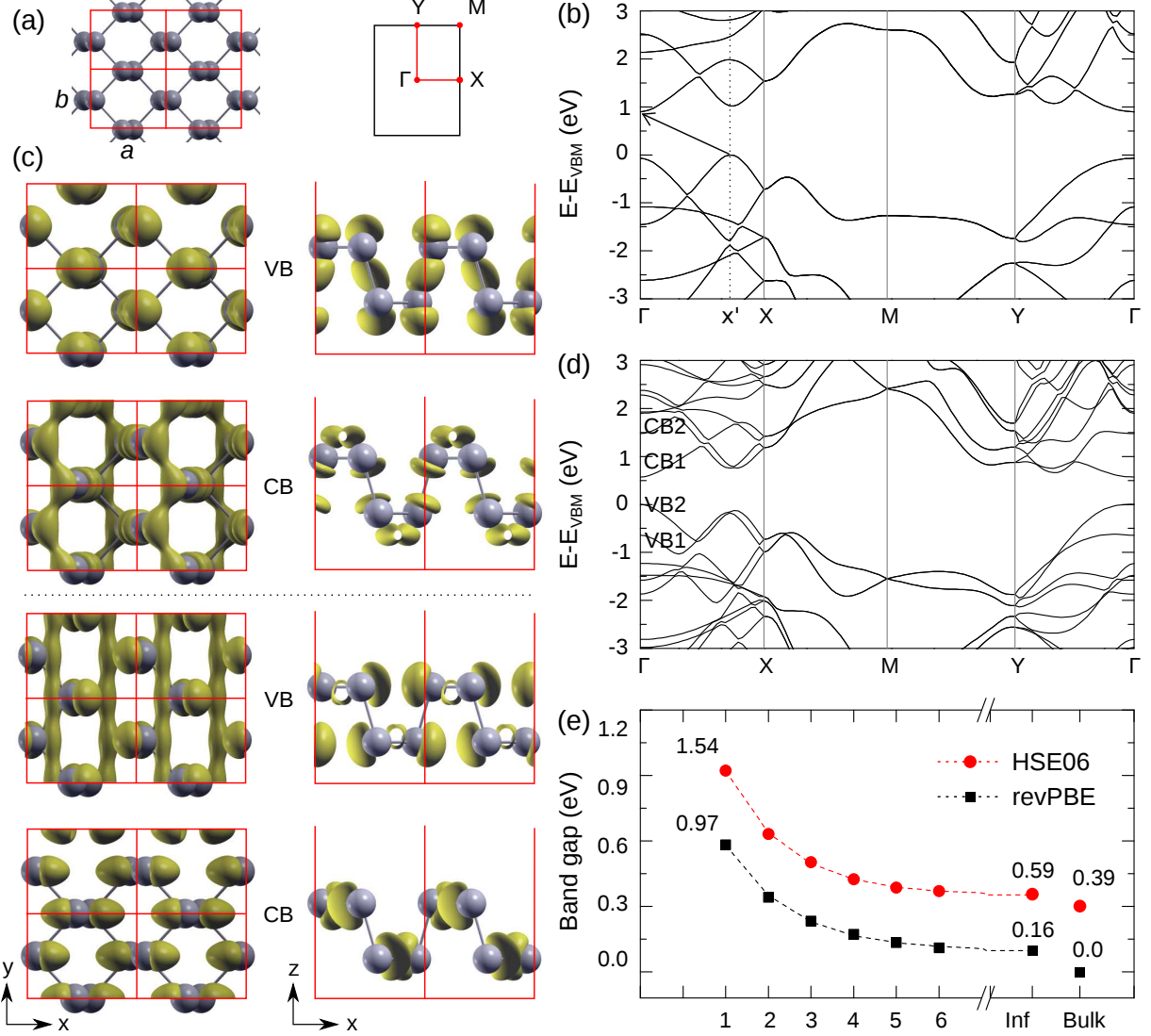


FIG. 2: (color online) (a) Top view of the monolayer arsenene and the associated Brillouin zone. (b) Band structures of monolayer arsenene. The arrow shows an indirect band gap. (c) Spatial wavefunctions of VBM and CBM at the  $\Gamma$  (top panel) and  $x'$  (labeled in b, bottom panel) points for monolayer arsenene. The isovalues are set to  $0.05 e\text{\AA}^{-3}$  (d) Band structure of bilayer arsenene. The bands VB1(2) and CB1(2) are labeled as well. (e) The fundamental band gaps as a function of the layer number at the  $\Gamma$  point. The bandgap values are marked for the monolayer system, for the extrapolation of our results and for the real bulk As. It should be noticed that the bandgap of monolayer is the direct value at the  $\Gamma$  point, not that as indicated by the arrow in (b). All results are obtained under the optimized structures with the revPBE-vdW functional.

TABLE I: The optimized lattice constants ( $a$ ,  $b$ , and  $c$ ) and structural parameters ( $R1, R2$ ,  $\theta1$ , and  $\theta2$ ) for the orthorhombic bulk As under five functionals. The corresponding values in experiment are given as well.

Functional	$a$ (Å)	$b$ (Å)	$c$ (Å)	$R1$ (Å)	$R2$ (Å)	$\theta1$ (°)	$\theta2$ (°)
Expt. [23]	4.47	3.65	11.00	2.48	2.49	98.5	94.1
PBE	4.67	3.71	11.45	2.51	2.52	99.89	95.08
revPBE-vdW	4.67	3.71	11.07	2.50	2.51	100.01	95.29
optPBE-vdW	4.38	3.72	10.91	2.49	2.50	98.03	96.30
optB88-vdW	4.26	3.73	10.88	2.48	2.49	97.29	96.83
optB86b-vdW	4.08	3.74	10.79	2.47	2.50	95.90	96.86

TABLE II: Carrier mobilities in few-layer arsenene. Types “e” and “h” denote the “electron” and “hole”, respectively.  $m_x^*$  ( $m_y^*$ ) (in unit of  $m_0$  with  $m_0$  being the static electron mass) represents the effective mass along the  $\Gamma$ -X (Y) direction.  $E_{1x}$  ( $E_{1y}$ ) (in unit of eV) is the deformation potential at  $\Gamma$  point along the  $\Gamma$ -X (Y) direction.  $C_{x-2D}$  ( $C_{y-2D}$ ) is the 2D elastic modulus for the  $\Gamma$ -X (Y) direction which is in unit of  $\text{Jm}^{-2}$ . Carrier mobility  $\mu_{x-2D}$  ( $\mu_{y-2D}$ ) (in unit of  $10^3 \text{ cm}^2\text{V}^{-1}\text{s}^{-1}$ ) along the  $\Gamma$ -X (Y) direction is calculated by using Eq. (1) together with  $T = 300 \text{ K}$ .

Type	$N_L$	$m_x^*/m_0$	$m_y^*/m_0$	$E_{1x}$	$E_{1y}$	$C_{x-2D}$	$C_{y-2D}$	$\mu_{x-2D}$	$\mu_{y-2D}$
e	1	0.23	1.22	0.81±0.17	3.74±0.04	28.99	74.69	5.29-12.32	0.17-0.18
	2	0.25	1.38	5.56±0.68	6.75±0.56	56.74	147.35	0.26-0.40	0.07-0.11
	3	0.23	1.39	3.67±0.21	5.21±0.12	83.98	218.55	0.92-1.16	0.21-0.23
	4	0.22	1.40	4.24±0.20	5.24±0.05	109.5	266.64	0.97-1.18	0.26-0.27
	5	0.19	1.41	5.13±0.17	5.38±0.11	136.90	362.37	1.06-1.21	0.35-0.38
	6	0.18	1.41	4.17±0.11	5.24±0.17	164.61	436.75	2.17-2.66	0.45-0.51
h	1	0.19	1.77	4.06±0.05	1.88±0.05	28.99	74.69	0.33-0.35	0.42-0.47
	2	0.21	4.49	1.96±0.24	2.01±0.06	56.74	147.35	1.13-1.89	0.13-0.14
	3	0.20	7.54	2.71±0.09	5.15±0.09	83.98	218.55	0.93-1.08	0.018-0.019
	4	0.20	10.08	2.43±0.04	5.53±0.05	109.53	266.64	1.35-1.44	0.012-0.013
	5	0.18	11.44	1.70±0.05	5.79±0.04	136.90	362.37	3.68-4.19	0.013-0.014
	6	0.16	11.44	3.09±0.21	6.36±0.11	164.61	436.75	1.49-1.94	0.014-0.015